A modified voltage changes ratio (MVCR) for in-vitro volume estimation

Una relación de cambio de voltaje modificada (MVCR) para estimación del volumen in-vitro

Víctor Hugo Mosquera-Leyton [iD] [1]* Carlos Felipe Rengifo-Rodas [iD] [1]

[1]Facultad de Ingeniería Electrónica y Telecomunicaciones, Universidad del Cauca. Calle 5 # 4-70. C. P. 190002. Popayán, Colombia.

UNIVERSIDAD DE ANTIOQUIA
1 8 0 3

Check for updates

ABSTRACT: Electrical bioimpedance (EBI) is a non-invasive technique for monitoring bladder volume. The EBI approaches global impedance (GI), impedance ratio method (IRM), and voltage change ratio (VCR) have been successfully applied to detect changes in the volume of objects with constant but unknown conductivity. In this work, simulated and in-vitro experiments are used to compare the performance of these methods with respect to a new approach proposed by some authors and called modified VCR (MVCR). Experimental results indicated that GI, VCR, and MVCR indices increase when the volume of the object under study increases. On the other hand, no direct or inverse relationship between IRM and volume was observed. The coefficient of variation, defined as the interquartile range divided by the median of a set of measurements, was lower for MVCR, which indicates that the proposed approach is less sensitive to measurement noise than the other three methods.

RESUMEN: La bioimpedancia eléctrica (EBI) es una técnica no invasiva para monitorear el volumen de la vejiga. Los índices EBI impedancia global (GI), método de relación de impedancia (IRM) y relación de cambio de voltaje (VCR) se han aplicado con éxito para detectar cambios en el volumen de objetos con conductividad constante pero desconocida. En este trabajo se utilizan experimentos simulados e in vitro para comparar el rendimiento de estos índices con respecto a un nuevo enfoque propuesto por algunos autores y denominado VCR modificado (MVCR). Los resultados experimentales indican que los índices GI, VCR, y MVCR se incrementan cuando aumenta el volumen del objeto estudiado. Por otro lado, no se observó una relación directa o inversa entre el IRM y el volumen. El coeficiente de variación, definido como el rango intercuartílico dividido por la mediana, fue menor para el MVCR, lo que indica que el enfoque propuesto es menos sensible al ruido de medición que los otros tres métodos.

1. Introduction

Spinal cord injuries cause complications of the urinary system such as flaccid neurogenic bladder and spastic bladder, which generate a lack of coordination between bladder contraction and sphincter relaxation. These dysfunctions cause urinary tract infections and kidney

stones due to loss of micturition sensation and vesicourethral reflux [1, 2]. The aim of urodynamics is to analyze bladder filling and emptying for the diagnosis of pathologies of the urinary system. Uroflowmetry is a medically approved technique for urodynamic studies that measure the volume of urine expelled per unit of time. This non-invasive method is complemented by ultrasound measurements to detect post-micturition urine residuals. The main disadvantage of uroflowmetry is that it cannot be applied to people with loss of micturition sensation [3]. Cystomanometry is another urodynamics approach that evaluates intravesical pressure variations

* Corresponding author: Victor Hugo Mosquera-Leyton

E-mail: mosquera@unicauca.edu.co

and the bladder volume through a catheter used to control bladder filling and to record intravesical pressure [4]. The drawback of Cystomanometry is its invasive nature. The most used procedure to help patients evacuate urine is urethral catheterization; however, it generates risks such as infections and kidney stones [5, 6]. For the previous reasons, it is necessary to use portable equipment to assist patients in determining bladder filling and avoid unnecessary catheterization due to the underestimation of bladder volume [5–7].

EBI is a promising method for monitoring tissue state and the functioning of organs in-vivo [8–10]; This technology is increasingly employed in the estimating and monitoring of bladder volume [11]. Schlebusch and collaborators [6, 7, 12] proposed the GI approach, which is linear and negatively correlated with bladder volume. The GI requires the reconstruction matrix that relates the pixels of an electrical impedance tomography (EIT) image with the estimated conductivity [13, 14]. GI is obtained by summing all pixel values of the image vector. Another alternative for volume estimation consists of the sum of orthonormal tetrapolar potential measurements obtained from electrodes located around a target area. Other alternatives for volume estimation consider the tetrapolar measurements obtained from electrodes located around a target area. According to [12] and [14], both IRM and VCR exhibit a high correlation between volume and the tetrapolar measurements of impedance and voltage, respectively. Unlike GI, these approaches do not require an image reconstruction algorithm.

IRM, proposed in [12], estimates the volume of an object by employing three impedance measurements. This approach presents a higher sensibility when the object under study is close to the boundary electrodes. It implies that the application of IRM to little objects located far from the boundary electrodes is limited [12]. On the other hand, VCR [14] requires two nonhomogeneous and one homogeneous measurement to determine impedance changes. IRM, unlike VCR, does not require these two types of measurements. The accuracy of IRM and VCR indexes is highly dependent on the location of the electrodes [11, 12]. The proposed MVCR approach employs redundant bioimpedance measurements based on the injection and measurement patterns proposed in [11], which are obtained by the system described in [15].

2. Mathematical background

In humans, each fluid and tissue have different electrical properties. EBI estimation is done by measuring the voltage signal generated by a constant amplitude alternating current injected through boundary electrodes [12]. In this work, the tetrapolar approach for EBI

measurement (Figure 1) is used to calculate the IRM, VCR, and MVCR indexes. On the other hand, the distribution of bioimpedance in a cross-section of the body is estimated using EIT (Figure 2). Then, GI index is calculated by adding the pixels of the EIT image [13, 14]. The GI, IRM, VCR, and MVCR are explained below.
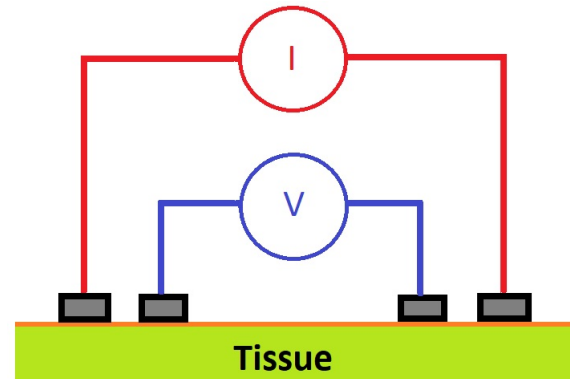

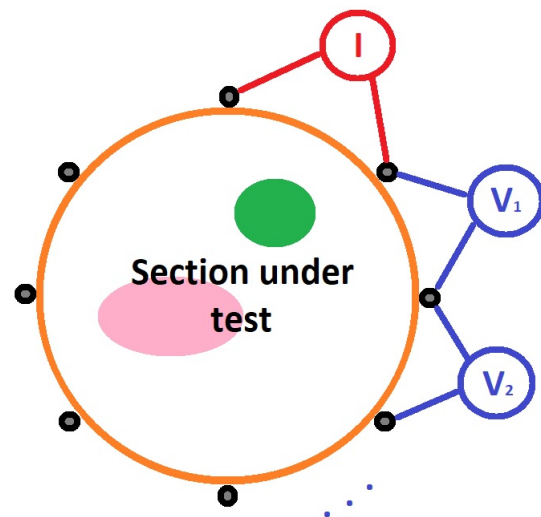**Figure 1** Tetrapolar approach for EBI measurement

Figure 2 Electrical Impedance Tomography approach

2.1 Global impedance (GI)

The GI requires images of differential EIT (dEIT) [14–16], in which homogeneous (v_h) and nonhomogeneous $\left(v_{nh}^f\right)$ vector measurements are considered, and differences between v_h and v_{nh}^f are used in a dEIT reconstruction algorithm to calculate changes of the conductivity inside the object under study [6, 12, 14]. The variations in the potential for any frame f (with a range from 1 to N_f) are calculated using Equation 1.

$$\Delta v^f(k) = \frac{v_{nh}^f(k) - v_h(h)}{v_h(h)}; k = 1, 2, \ldots N \qquad (1)$$

$\Delta v^f(k), v_{nh}^f(k)$, and $v_h(h)$ the k-th element of the vectors $\Delta v^f, v_{nh}^f$, and v_h respectively, and N is the number of voltage measures per frame. The pixel conductivity vector I^f, and the matrix R^f are calculated using the Graz algorithm for EIT (GREIT), which it is the most accepted for researchers to image reconstruction of dEIT [17]. R^f has M rows (number of pixels of the conductivity image) and N columns. Hence, the vector I^f and v^f are related by Equation 2.

$$I^f = R^f \Delta v^f \qquad (2)$$

The dimensionless GI is calculated by adding the values of all I^f pixels for each frame (Equation 3).

$$GI = \sum_{f=1}^{N_f} \sum_{k=1}^{N} I^f(k) \qquad (3)$$

Considering that the measurement system had eight ports and because voltages at the three electrodes are not measured (injection electrode, drain electrode, and the nearest neighbor of the injection electrode), each frame contains N=40 voltages measurements. The GI is calculated from a 2D dEIT image of 32 by 32 pixels, using a finite element model of 37,412 elements implemented in *Electrical Impedance and Diffuse Optical Tomography Reconstruction Software* (EIDORS).

2.2 Impedance ratio method (IRM)

IRM relates volume to change in impedance. This technique estimates volumes independently of the conductivity of the object under study. The three tetrapolar measurements required to calculate the impedance ratio are presented in Figure 1 [12]. The frontal measurement is used to calculate $Z_f = \frac{V_f}{I_f}$ the backward measurement defines $Z_b = \frac{V_b}{I_b}$ and the side measurement determines $Z_s = \frac{V_s}{I_s}$. According to [12], the greatest sensibility to impedance variations is obtained when the object under study is close to the contour electrodes because, in such a configuration, current densities are maximized. Therefore, increasing the volume of the object implies a greater change in the sensitivity of impedance measurements. IRM is defined by Equation 4.

$$IRM = \frac{Z_s - Z_f}{Z_b - Z_f} \qquad (4)$$

2.3 Voltage changes ratio (VCR) and Modified VCR

VCR associates the voltage change with the volume of the object under study [11]. This is calculated considering one reference measurement (V_0) and one perturbed measurement (V) (Equation 5). The first is obtained when
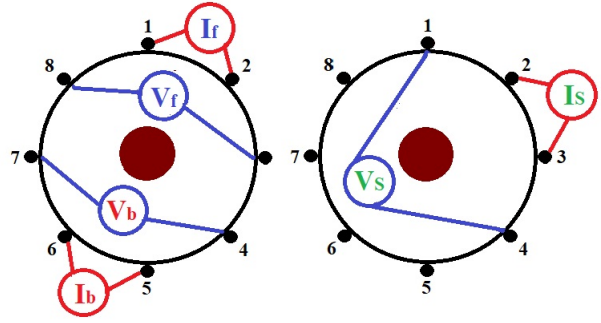

Figure 3 Injection and measurement of signals for IRM

the studied object has the lowest volume, while the second is when this object has its highest volume

$$VCR = \frac{|V - V_0|}{V_0} \qquad (5)$$

The electric potentials are measured considering the configuration shown in Figure 2.
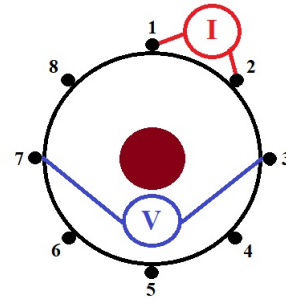

Figure 4 Injection and measurement of signals for VCR

To reduce noise sensitivity, we propose to estimate volume using eight voltage measurements instead of one, and use the patterns indicated in Figure 3.
The MVCR index is calculated by Equation 6.

$$MVCR = \frac{1}{8} \sum_{i=1}^{8} \frac{|V_i - V_0|}{V_0} \qquad (6)$$

In the above equation, V_0 is the voltage obtained when the current is injected through electrodes 1 and 2, and the studied object has the lowest volume. Like VCR, the voltages $V_i (i = 1...8)$ are the potentials when the object is at its final volume (Figure 3). Equations 3, 4, 5 and 6 show that IRM, VCR, and MVCR are dimensionless, just like GI.

3. Materials and methods

3.1 Measurement system

The experimental results presented in this study were obtained using an EIT system based on the AFE4300
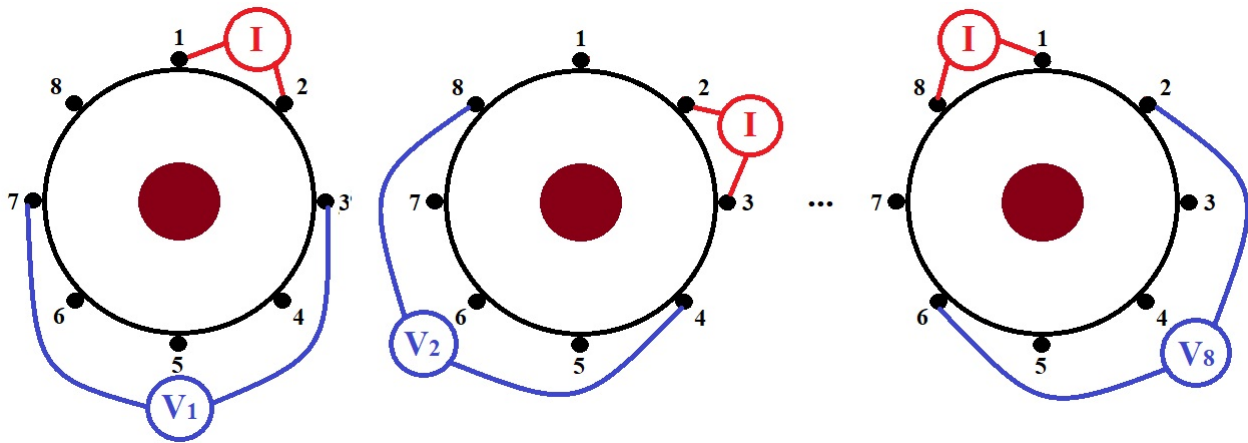
Figure 5 Injection and measurement of signals for MVCR

analog front-end of Texas Instruments. This integrated circuit has eight ports for current injection and potential measurement [15]. The AFE4300 generates an alternating current of 50 kHz and 294.5 µArms through a voltage-controlled current source (VCC). The alternating signal is generated by an internal direct digital synthesizer (DSS) and a 6-bit and 1-MHz digital-to-analog converter (DAC). The potentials at the electrodes are measured by a demodulator, which can be configured to obtain only the amplitude of the sinusoidal signal (full-wave rectifier (FWR) mode) or the in-phase and quadrature (I/Q) components. Our experiments used the FWR mode because it is faster than the I/Q mode. The amplitudes are quantized to 16-bits using a delta-sigma analog-to-digital converter (ADC) with a clock frequency of 1 MHz [18]. The AFE4300 is connected to a PIC16F886 microcontroller, which in turn receives the injection and measurement patterns from a LabVIEW application through an HC06 Bluetooth module. The EBI system has a protection network composed of resistors and capacitors that eliminates the DC offset present in the current signals. The power to the EBI system is supplied by a 3.7V lithium polymer (LiPO) battery. The protection network, the current amplitude (294.5 μA_{rms}), and the LiPO power supply make this device compliant with the safety standard IEC60601 for medical equipment. Figure 4 shows the block diagram of the EIT system.

The injection and measurement patterns are configured through the ISWMUX and VSENSEMUX registers of the AFE4300 [19].

3.2 The environment of experimentation

Simulation experiments

The first part of the present study was carried out through a finite element simulation, in which the bladder was
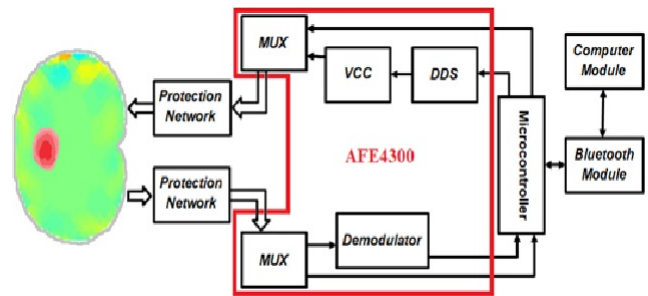

Figure 6 EBI system diagram

represented by a sphere whose radius varied from 0.05 to 0.19 m with increments of 0.01 m. (Figure 5). A ring of 8 electrodes was used to simulate current injection and the measurement of potentials. A previous work [20] shows details of this experiment.
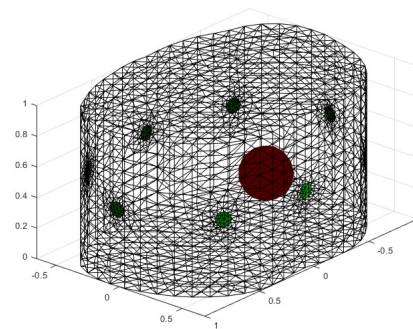

Figure 7 Finite element model of the lower pelvis [20]

In-vitro experiments

The in vitro experiments were performed in a cylindrical phantom with a radius of 15 cm and a height of 30 cm, which

was filled with a 4 g/L saline solution. The 8 electrodes were symmetrically distributed around a ring surrounding the phantom. To simulate the bladder, three steel spheres with volumes of 0.028 $m^3, 0.030m^3, and 0.0314m^3$ were placed one by one into the phantom. The center of each sphere was aligned with the center of the electrode ring. Also, the equator of the sphere and the ring of electrodes were in the same plane (Figure 6). For each sphere, 30 voltage measurements were taken. The three data sets, one for each sphere, were used as the inputs for the volume estimation methods GI, IRM, VCR, and MVCR. For each method, the medians of the three data sets were compared with each other using the nonparametric Kruskal-Wallis test. This approach was used instead of an ANOVA test because of the non-normality of the data.
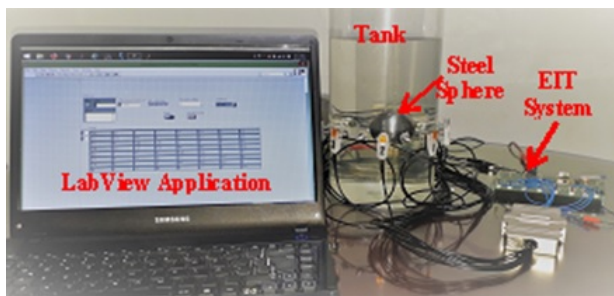

Figure 8 Assembly of the saline phantom

4. Results

4.1 Simulations of volume estimation

Figure 9 shows that IRM has the lowest accuracy when compared to $|GI|^{-1}$, VCR, and MVCR. The studies [11, 14, 15] show that both GI and VCR have good accuracy in the volume estimation of in-vivo experiments, which is consistent with the simulation results presented in Figures 9a, 9c, and 9d. The GI obtained the lowest error $(-4.6E - 4)$, followed by MVCR $(1.8E - 3)$ and VCR $(2.2E - 3)$. These values indicate that the proposed MVCR is a viable alternative for volume monitoring since, in addition to having a low error, it does not require computationally expensive image reconstruction algorithms, as is the case with GI.

4.2 In-vitro results

The performance of GI, IRM, VCR, and MVCR was evaluated using a cylindrical phantom and three steel spheres: small, medium, and large, with radii of 27.5, 35.0, and 37.5 mm, respectively. For each trial, only one sphere was placed in the tank. The Kruskal-Wallis test was used to determine whether the differences between measurements were statistically significant. Figures 10

to 13 show the box plot considering 30 measurements for each sphere. The dispersion of the data is caused by the electromagnetic interference resulting from coupling the system with the phantom since the metal-electrolyte interface generates spontaneous voltage fluctuations [21]. For each of the four indices compared in this study, medians, interquartile ranges, and coefficient of variation are presented in Tables 1 and 2. The p-values from Kruskal-Wallis test for differences between the medians of the estimated volumes are presented in Table 3. The differences were considered statistically significant when p < 0.05, which indicates the possibility of distinguishing between the three spheres.

Schlebusch and collaborators [7] show that GI is inversely proportional to the volume of the object. In this work, the linear relationship between $|GI|^{-1}$ and volume was confirmed for the in-vitro experiments (Figure 10). The interquartile ranges, which were lower than $3.5E - 4$, reveal the low sensitivity of $|GI|^{-1}$ to measurement noise (Table 1). In addition, the Kruskal-Wallis test (Table 3) confirmed that the difference between the $|GI|^{-1}$ values for each sphere was significant $(p = 1.34E - 8)$. These results are not in agreement with [13], where the researchers found that the GI has a reduced sensitivity to volume changes when a ring arrangement of electrodes is used. Therefore, our results suggest that $|GI|^{-1}$ is a viable alternative for volume monitoring using 8 electrodes in a simple ring configuration, and adjacent patterns for injection and measurement.

Table 1 Medians and interquartile ranges of measurements for each volume estimation method and sphere size

		Small	Medium	Large
Median	**GI**	2.88E-2	3.03E-2	3.14E-2
	IRM	47	1.12	2.91
	VCR	2.68	3.69	6.09
	MVCR	1.33	1.36	1.38
Interquartile ranges	**GI**	1.70E-02	3.04E-02	3.50E-02
	IRM	76	0.17	0.95
	VCR	0.09	0.18	0.21
	MVCR	3.00E-02	3.50E-02	4.20E-03

Table 2 Coefficient of variation for each volume estimation method and sphere size

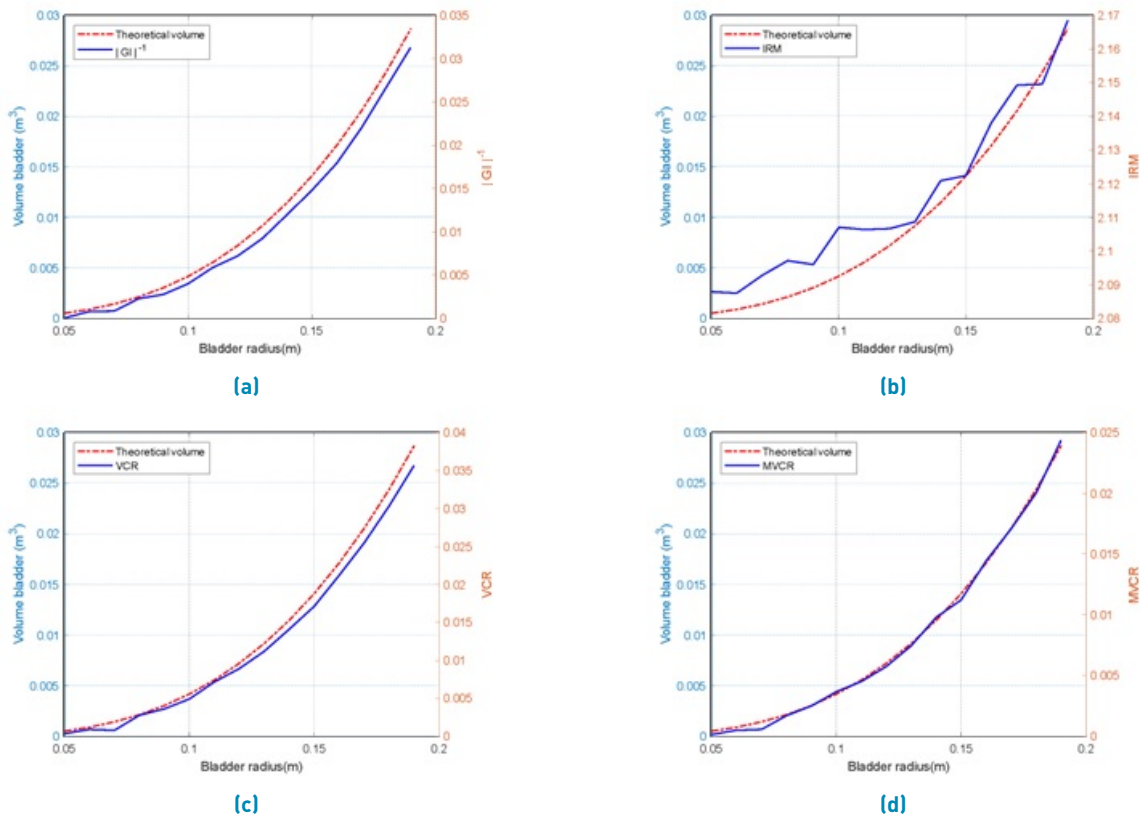|	GI	IRM	VCR	MVCR
Small	5.90E-1	1.61	3.35E-2	2.26E-3
Medium	0.10E-1	0.15	4.87E-2	2.57E-3
Large	0.11E-1	0.32	3.44E-2	3.04E-3

(a)

(b)

(c)

(d)

Figure 9 Simulation results for a) $|GI|^{-1}$, b) IRM, c) VCR, and d) MVCR
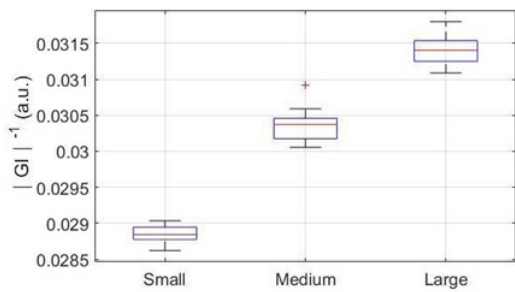

Figure 10 GI results for volume variation
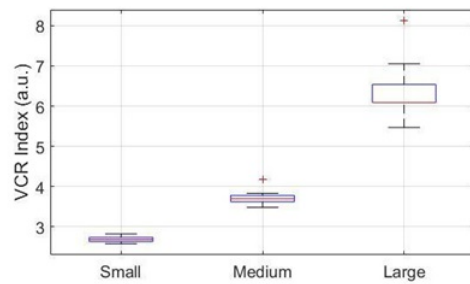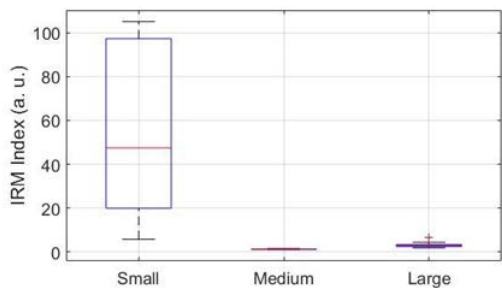

Figure 12 VCR results for volume variation

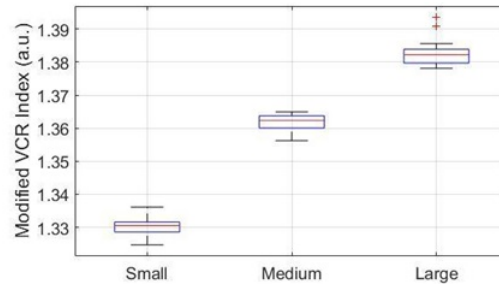**Figure 11** IRM results for volume variation

Figure 13 MVCR results for volume variation

Table 3 p-values from Kruskal-Wallis test for each index and sphere size

	Small-Medium	Medium-Large	Small-Large
GI	1.34E-8	1.34E-8	1.34E-8
IRM	2.26E-7	2.26E-7	1.04E-7
VCR	1.24E-8	1.11E-8	1.10E-8
MVCR	1.32E-8	1.32E-8	1.32E-8

Figure 11 shows the results of the IRM approach. The median values of the IRM measurements are different for the three spheres (Table 1). Table 1 shows that the medium-sized sphere has the lowest median (1.12), while the small sphere has the largest median (47). These results corroborate the limitation of IRM for small volume estimation, as indicated in [12]. These results make IRM unsuitable for bladder volume estimation.

Figures 12 and 13 show that for VCR and MVCR, the measurements of the spheres do not overlap, and Table 3 indicates that the median values for these approaches are significantly different for the three spheres. The proposed MVCR is an extension of the VCR that uses eight voltage measurements to reduce noise sensitivity. As can be seen from Tables 1 and 2, the quotient between the interquartile range and the median (coefficient of variation) is lower for MVCR (Table 2), which indicates that the proposed approach improves precision.

The interquartile ranges for $|GI|^{-1}$, VCR, and MVCR (Table 1) show that it is feasible to discriminate between the three spheres. For the four methods, the Kruskal-Wallis test (Table 3) indicates that the differences between the medians of the estimates are significant. However, as presented in Table 1, there is no direct or inverse relationship between IRM medians and the volume of the spheres.

Of the four approaches contemplated in this study, $|GI|^{-1}$ has the lowest sensitivity to volume change, since, as indicated in Table 1, the variation between the medians of the three spheres is on the order of thousandths. On the other hand, VCR has the highest sensitivity to volume change, and MVCR has a volume sensitivity greater than GI and less than VCR (Table 1). MVCR has the lowest coefficient of variation (Table 1). These results show that MVCR is the best alternative for volume monitoring.

The bioimpedance approaches (VCR, IRM, and MVCR) are used to detect changes in volume when the object conductivity under study remains constant, using only the potential measurements. Furthermore, these methods require less computational effort than the $|GI|^{-1}$ approach, which requires solving the EIT inverse problem. In this study, the in-vitro performance of volume estimation indices based on constant conductivity and variable volume objects was analyzed. The effects of conductivity variation will be considered in subsequent studies, as well as in-vivo analysis of the GI, VCR, and MVCR approaches.

5. conclusions

The results obtained with the steel spheres and the saline solution show that $|GI|^{-1}$, VCR, and MVCR are suitable approaches for volume monitoring when the conductivity of the object under study is unknown but constant. VCR had the highest sensitivity to volume variation, while MVCR had a small interquartile rank. Both VCR and MVCR are simpler to implement than $|GI|^{-1}$ because they do not require image reconstruction algorithms. These results show the viability of doing long in-vivo volume estimation experiments using an EIT system with 8 electrodes and the MVCR approach.

6. Declaration of competing interest

We declare that we have no competing interests, including financial or non-financial, professional, or personal interests interfering with the full and objective presentation of the work described in this manuscript.

7. Acknowledgements

8. Funding

9. Author contributions

Mosquera-Leyton developed the experiments for data collection and the development of the EIDORS-Matlab application to obtain the indices under analysis. Rengifo-Rodas performed the data analysis, both authors wrote the paper.

10. Data availability statement

Data sets obtained for each experiment are available and can be requested from the authors.

References

[1] W. A. Taweel and R. Seyam, "Neurogenic bladder in spinal cord injury patients," *Research and Reports in Urology*, vol. 7, Jun. 10, 2015. [Online]. Available: https://doi.org/10.2147/RRU.S29644

[2] N. Yoshimura and M. B. Chancellor, "Differential diagnosis and treatment of impaired bladder emptying," *Reviews in urology*, vol. 6, no. 1, 2004. [Online]. Available: https://www.ncbi.nlm.nih.gov/pmc/articles/PMC1472851/

[3] W. Schafer, P. Abrams, L. Liao, A. Mattiasson, F. Pesce, and *et al.*, "Good urodynamic practices: Uroflowmetry, filling cystometry, and pressure-flow studies," *Neurourology and Urodynamics*, vol. 21, no. 3, 2002. [Online]. Available: https://doi.org/10.1002/nau.10066

[4] E. Martínez-Agulló, J. P. Burgués-Gasión, and J. M. Alapont-Alacreu, "Vejiga neurógena. conceptos básicos," *Cínicas Urológicas de la complutense*, vol. 8, 2000. [Online]. Available: https://dialnet.unirioja.es/servlet/articulo?codigo=2039159

[5] M. A. Lindozo-Lopes and E. D. R. de Paula Lima, "Continuous use of intermittent bladder catheterization - can social support contribute?" *Rev. Latino-Am. Enfermagem*, vol. 22, no. 3, May-Jun. 2014. [Online]. Available: https://doi.org/10.1590/0104-1169.3268.2438

[6] T. Schlebusch, S. Nienke, S. Leonhardt, and M. Walter, "Bladder volume estimation from electrical impedance tomography," *Physiological Measurement*, vol. 35, no. 9, Aug. 20, 2014. [Online]. Available: https://doi.org/10.1088/0967-3334/35/9/1813

[7] T. Schlebusch and S. Leonhardt, "Effect of electrode arrangements on bladder volume estimation by electrical impedance tomography," *Journal of Physics: Conference Series*, vol. 434, Apr. 2013. [Online]. Available: https://doi.org/10.1088/1742-6596/434/1/012080

[8] M. Min and T. Parve, "Improvement of lock-in electrical bio-impedance analyzer for implantable medical devices," *IEEE Transactions on Instrumentation and Measurement*, vol. 56, no. 3, Jun. 2007. [Online]. Available: https://doi.org/10.1109/TIM.2007.894172

[9] S. Hersek, H. Toreyina, C. N. Teague, M. L. Millard-Stafford, H. K. Jeong, and *et al.*, "Wearable vector electrical bioimpedance system to assess knee joint health," *IEEE Transactions on Biomedical Engineering*, vol. 64, no. 10, Oct. 2017. [Online]. Available: https://doi.org/10.1109/TBME.2016.2641958

[10] M. Grossi and B. Riccó, "Electrical impedance spectroscopy (eis) for biological analysis and food characterization: a review," *Journal of Sensors and Sensor Systems*, vol. 6, no. 2, Aug. 28, 2017. [Online]. Available: https://doi.org/10.5194/jsss-6-303-2017

[11] Y. Li, Y. Peng, X. Yang, S. Lu, J. Gao, and *et al.*, "Analysis of measurement electrode location in bladder urine monitoring using electrical impedance," *Journal of Sensors and Sensor Systems*, vol. 18, no. 34, Mar. 22, 2019. [Online]. Available: https://doi.org/10.1186/s12938-019-0651-4

[12] T. Schlebusch, J. Orschulik, J. Malmivuo, S. Leonhardt, D. Leonhauser, and *et al.*, "Impedance ratio method for urine conductivity-invariant estimation of bladder volume," *Journal of Electrical Bioimpedances*, vol. 5, no. 1, Jan. 2014. [Online]. Available: https://doi.org/10.5617/jeb.895

[13] D. Leonhauser, C. Castelar, T. Schlebusch, M. Rohm, R. Rupp, and *et al.*, "Evaluation of electrical impedance tomography for determination of urinary bladder volume: comparison with standard ultrasound methods in healthy volunteers," *BioMedical Engineering OnLine*, vol. 17, no. 95, Jul. 13, 2018. [Online]. Available: https://doi.org/10.1186/s12938-018-0526-0

[14] S. Leonhardt, A. Cordes, H. Plewa, R. Pikkemaat, I. Soljanik, and *et al.*, "Electric impedance tomography for monitoring volume and size of the urinary bladder," *De Gruyter*, Nov. 22, 2011. [Online]. Available: https://doi.org/10.1515/BMT.2011.022

[15] V. H. Mosquera, R. Bragós, A. Arregui, and C. F. Rengifo, "Implementation of a low cost prototype for electrical impedance tomography based on the integrated circuit for body composition measurement afe4300," presented at Proceedings of the 11th International Joint Conference on Biomedical Engineering Systems and Technologies - BIODEVICES, Madeira, Portugal, 2018.

[16] C. Castelar, "Internal electrode bladder volume eit for routine urodynamic test application: An fem study using eidors framework," presented at Proceedings of the 20th International Scientific Student Conference Poster, Prague, Czech, 2016.

[17] B. H. Brown, "Electrical impedance tomography (eit): a review," *Journal of Medical Engineering & Technology*, vol. 27, no. 3, Jul. 09, 2009. [Online]. Available: https://doi.org/10.1080/0309190021000059687

[18] V. Yang, P. Aroul, and K. Wen, "Impedance measurement with the afe4300," Texas Instruments, Dallas, Texas, Tech. Rep. SBAA202, Oct. 2013.

[19] S. Madushan, "Low-cost, integrated analog front-end for weight-scale and body composition measurement check for samples: Afe4300," Texas Instruments, Dallas, Texas, Tech. Rep. SBAS586B, Jun. 2012.

[20] J. D. M. Sánchez, V. H. M. Leyton, and C. F. R. Rodas, "Effect of the injection and measurement patterns and the geometric distribution of electrodes in bladder volume estimation using electrical impedance tomography," presented at XXIII Symposium on Image, Signal Processing and Artificial Vision (STSIVA), Popayan, Colombia, 2021.

[21] D. Naranjo-Hernández, J. Reina-Tosina, and M. Min, "Fundamentals, recent advances, and future challenges in bioimpedance devices for healthcare applications," *Journal of Sensors*, vol. 2019, Jul. 15, 2019. [Online]. Available: https://doi.org/10.1155/2019/9210258